 CMES, vol.39, no.2, pp.101-123, 2009

Simulation of high explosive explosion using adaptive material point method

Shang Ma [1], Xiong Zhang [1 2], Yanping Lian [1] and Xu Zhou[3]

Abstract: Numerical simulation of high explosive explosion problems is a big challenge to traditional numerical methods because explosion usually involves extremely large deformation and multi-material interaction of different phases. Recently developed meshfree methods show much advantages over mesh-based method for problems associated with very large deformation. Some of them have been successfully applied to impact and explosion problems, such as smoothed particle hydrodynamics (SPH). Similar to SPH, material point method (MPM) is an efficient meshfree particle method solving continuum problems. With combination of the advantages of Eulerian and Lagrangian methods, MPM is a promising numerical tool for solving large deformation problems, such as high explosive detonation and consequent demolishment to the structures. A three dimensional MPM code, MPM3DPP, is developed by using C++ programming language. With adaptive particle splitting scheme proposed in this paper, MPM3DPP is capable of simulating different explosion problems. Johnson-Cook material model is implemented in order to take strain rate effect and thermal softening effect into consideration. Mie-Grüneisen equation of state is used to treat volumetric response of metal under high pressure. Jones-Wilkins-Lee (JWL) equation of state is used for describing the expansion process of detonation products. Artificial viscosity is added to pressure term to stabilize and capture the shock wave. The MPM3DPP code is validated by simulating TNT slab detonation and shock tube problem, and then is used to simulate different explosion problems including explosively driven flyer problem and shaped charge problem. The computational results are in good agreement with empirical formula and experimental results.

Keywords: Material point method, Adaptive, High explosive, Numerical simulation, Meshless

[1] School of Aerospace, Tsinghua University, Beijing, P. R. China
[2] Corresponding author: xzhang@tsinghua.edu.cn
[3] Beijing Institute of Special Engineering Design and Research, P. R. China

1 Introduction

The explosion of high explosive generates extreme high pressure and leads to severe interaction between gaseous products and surrounding materials in a very short time range. Behavior of explosion is complicated and usually involves extreme large deformation and multi-material interaction of different phases [[43]]. With the development of computer hardware, numerical simulation plays more and more important roles in engineering applications of high explosive. Shaped charges, for example, have many useful applications in defense industry and in oil industry for penetrating hard targets such as armor, tanks, rocks or concrete walls. There are numerous parameters, such as liner thickness or cone angle, should be considered in shaped charge design. Effective numerical simulation is useful in saving experimental cost. However, the numerical simulation of high explosive detonation and the product expansion is difficult for traditional numerical methods due to the shock wave involved in detonation and extreme large deformation in consequent process. Eulerian method avoids mesh distortion but additional effort have to be made to track the interface and eliminate the numerical diffusion and dissipation. With fixed mesh, Eulerian hydrocodes are capable of handling extreme large deformation involved in both detonation and jet formation process, and are extensively used in shaped charge design [[19, 10]]. Specific material interface tracking technique, such as level set method [[40]], fuzzy interface treatment [[32]], Youngs interface reconstruction method [[27]], should be used to track the material interface in Eulerian methods. Leaving aside the mesh distortion problem, Lagrangian methods are still attractive for their ability of simulating history dependent material and tracking the material interface. However, traditional mesh-based Lagrangian method, such as finite element method, suffered from mesh distortion and element entanglement. Effort must be taken to design remeshing algorithm [[30]]. Arbitrary Lagrangian-Eulerian (ALE) can be an alternative for high explosive simulation [[1]]. The major numerical difficulty lies in ALE is designing an effective mesh moving algorithm for a three-dimensional complicated material domain. Furthermore, the numerical diffusion and dissipation are still exist in ALE method.

Recently developed meshless methods [[7, 20, 2]] show much advantages over mesh-based method for problems associated with very large deformation. Some of them have been successfully applied to impact and penetration problems [[18, 14]]. Smoothed particle hydrodynamics(SPH) has been used to simulate fragmentation of cased explosives [[34]] and the detonation process of unlined shaped charge [[21]]. It was shown that meshfree particle methods are very natural for such problems.

Material point method (MPM) [[37, 39]] is a particle method for solving continuum problems. It is an extension of particle-in-cell(PIC) [[9]] method to solid mechan-

ics. Recently, a generalized formulation was developed based on Petrov-Galerkin discretization scheme and was named as Generalized Interpolation Material Point (GIMP) method [[6]], of which original MPM is a special case. GIMP method provides better accuracy and stability with the smoother grid basis function. Compared with other meshless methods, GIMP method and Meshless Local Petrov-Galerkin (MLPG) method [[3, 15]] are both Petrov-Galerkin based methods and have a lot in common. Each of them consist of a family of methods. The differences lie in background mesh. MLPG method is fully meshless method without using any kind of computational mesh. GIMP method make use of background mesh to calculate differentiation and solve equations of motion.

In MPM/GIMP, the material points provide a Lagrangian description of the material. Mass, position, velocity and stress, as well as material parameters and internal variables needed for constitutive models are carried by material points. Background mesh with Eulerian description is used for solving the momentum equations. Usually a regular Cartesian lattice that covers the computational domain is used as background mesh. With combination of the advantages of Eulerian and Lagrangian methods, MPM is a suitable numerical tool for large deformation problems. MPM and its variant have been applied in diverse problems such as impact [[39, 42]], fracture [[12, 11]], metal forming [[38]], granular media [[4]], blast induced fragmentation [[16]] and multiscale problem [[25, 23]]. MPM also showed some advantages over SPH in efficiency and stability for hypervelocity problems [[26]].

However, the numerical fracture may occur when two particles are separated by a grid cell in MPM simulation [[42]]. Therefore, in some cases that the deformation is very large, such as expansion of explosion product and extreme stretch of the liner material, MPM may not give right solution without particle rearrangement or particle adding scheme. In this paper, adaptive particle splitting scheme is proposed in order to improve the simulation capability of MPM. Particle is split into two particles when its accumulative strain in one direction exceed the specified criterion, which indicate particle is stretched the most in that direction.

A three dimensional MPM code with adaptive particle splitting, MPM3DPP, is developed by using C++ programming language. Johnson-Cook material model is implemented in order to take strain rate effect and thermal softening effect into consideration. Mie-Grüneisen equation of state is used to treat volumetric response of metal under high pressure. Jones-Wilkins-Lee(JWL) equation of state is used for describing the expansion process of detonation products. Artificial viscosity is added to pressure term to stabilize and capture the shock wave.

This paper is organized as follows. A brief description of the material point method is provided in section 2. The adaptive splitting scheme of material point is given

in the next section. Numerical implementation of material model, equation of state and artificial bulk viscosity are described in section 4. Several numerical examples, including TNT slab detonation, shock tube, and jet formation are illustrated in section 5. Finally, concluding remarks are presented in the last section.

2 Material point method

2.1 Basic Formulation

The material domain is discretized by a finite number of particles in MPM. The solution process of MPM is divided into two phases. In the first phase of solution, particles are rigidly attached to the background grid and they deform with the grid. After obtaining the kinematic solution on the grid nodes, they are mapped back to the particles to update their positions and velocities. The deformed grid is discarded in the subsequent time step and a new regular grid is used to avoid mesh distortion. For continuum, material is governed by the momentum equations [[13]]

$$\sigma_{ij,j} + \rho f_i = \rho \ddot{u}_i \quad \forall x_i \in V \tag{1}$$

subject to the traction boundary conditions

$$\sigma_{ij} n_j = t_i(t) \quad \forall x_i \in \Gamma_t \tag{2}$$

and the displacement boundary conditions

$$u_i(X_\alpha, t) = d_i(t) \quad \forall x_i \in \Gamma_d \tag{3}$$

where V is the current material domain, Γ_t and Γ_d are respectively the boundary portions of V prescribed with traction and displacement, σ_{ij} is the Cauchy stress, ρ is the current density, f_i is the body force density, $\ddot{u}_i$ is the acceleration, the comma denotes covariant differentiation and n_j is the unit outward normal to the boundary. The fundamental formulation of MPM can be obtained from the weak form of momentum equations and traction boundary condition as:

$$\begin{aligned}\delta\Pi = &\int_V \rho \ddot{u}_i \delta u_i \mathrm{d}V + \int_V \rho \sigma^s_{ij} \delta u_{i,j} \mathrm{d}V \\ &- \int_V \rho f_i \delta u_i \mathrm{d}V - \int_{\Gamma_t} t_i \delta u_i \mathrm{d}\Gamma = 0\end{aligned} \tag{4}$$

where $\sigma^s_{ij} = \sigma_{ij}/\rho$ is the specific stress. The energy equation is given by

$$\dot{E} = J\sigma_{ij}\dot{\varepsilon}_{ij} = Js_{ij}\dot{\varepsilon}_{ij} - Jp\dot{\varepsilon}_{kk} \tag{5}$$

where J is the determinant of the deformation gradient matrix $F_{ij} = \partial x_i / \partial X_j$, E is the energy per unit initial volume. $\dot{\varepsilon}_{ij}$ is the strain rate, s_{ij} and p represent the deviatoric stresses and pressure, i.e. $s_{ij} = \sigma_{ij} + p\delta_{ij}$.

Because the particles are rigidly attached to the computational grid, the particle displacement u_{pi} and its derivatives $u_{pi,j}$ can be obtained by mapping their grid point values u_{gi} and $u_{gi,j}$ to the particle using the standard finite element shape functions of the grid, namely

$$u_{pi} = \sum_{g=1}^{8} N_{gp} u_{gi} \tag{6}$$

$$u_{pi,j} = \sum_{g=1}^{8} N_{gp,j} u_{gi} \tag{7}$$

where $N_{gp} = N_g(x_{pi})$. For three dimensional cases, 8-point hexahedron grid is used as the background grid so that the shape function is given by

$$N_g = \frac{1}{8}(1+\xi\xi_g)(1+\eta\eta_g)(1+\zeta\zeta_g), \quad g = 1,2,\cdots 8 \tag{8}$$

if the particle (ξ, η, ζ) is inside the hexahedron, where ξ_g, η_g and ζ_g take on their nodal values (± 1, ± 1, ± 1) at the grid node g. If the particle is outside the hexahedron, $N_g = 0$.

The material mass is lumped at particles, hence the density ρ at point x_i can be approximated as

$$\rho(x_i) = \sum_{p=1}^{n_p} M_p \delta(x_i - x_{pi}) \tag{9}$$

where x_{pi} denotes the coordinate of pth particle in ith direction. Since the movement of particles represents the deformation of physical domain and mass is carried by particles, the mass conservation is automatically satisfied in MPM.

Substituting Eqs. (6), (7) and (9) into the weak form (4), and invoking the arbitrariness of δu_{hi} yields

$$\dot{p}_{hi} = f_{hi}^{\text{int}} + f_{hi}^{\text{ext}}, \quad h = 1,2,\cdots,n_g \tag{10}$$

where n_g is the number of grid nodes,

$$p_{hi} = \sum_{g=1}^{n_g} m_{hg} \dot{u}_{gi} \tag{11}$$

is the momentum of hth grid point in the ith direction, $m_{hg} = \sum_{p=1}^{n_p} M_p N_{gp} N_{gp}$ is the mass matrix. The lumped mass matrix is used in common explicit methods [[8]] and in practical explicit material point method [[24]]. By using lumped mass matrix $m_h = \sum_{p=1}^{n_p} M_p N_{hp}$, the momentum p_{hi} can be simplified as

$$p_{hi} = m_h \dot{u}_{hi} \tag{12}$$

Moreover,

$$f_{hi}^{\text{int}} = -\sum_{p=1}^{n_p} V_p N_{hp,j} \sigma_{pij} \tag{13}$$

and

$$f_{hi}^{\text{ext}} = \sum_{p=1}^{n_p} M_p N_{ph} f_{pi} + \sum_{p=1}^{n_p} M_p N_{hp} t_{pi}^s h^{-1} \tag{14}$$

are the internal force and external force, $t_{pi}^s = t_{pi}/\rho$ is the specific traction, h is the thickness of the boundary layer, $\sigma_{pij} = \sigma_{ij}(x_p)$ and $f_{pi} = f_i(x_p)$.

Explicit time integration is used. The momentum equations on gride nodes can be integrated as

$$p_{hi}^{k+1} = p_{hi}^k + (f_{hi}^{\text{int}} + f_{hi}^{\text{ext}})\Delta t \tag{15}$$

where the superscripts "k" and "$k+1$" denote the values at time t^k and t^{k+1}, respectively. The particle velocities and positions are updated by

$$x_{pi}^{k+1} = x_{pi}^k + \sum_{h=1}^{n_g} \frac{p_{hi}^{k+1}}{m_h^k} N_{hp}^k \Delta t \tag{16}$$

$$v_{pi}^{k+1} = v_{pi}^k + \sum_{h=1}^{n_g} \frac{f_{hi}^k}{m_h^k} N_{hp}^k \Delta t \tag{17}$$

where $f_{hi}^k = f_{hi}^{\text{int}} + f_{hi}^{\text{ext}}$.

Jaumann rate is used to ensure the objectivity of the stress, namely

$$\dot{\sigma}_{ij} = \sigma_{ij}^{\nabla} + \sigma_{jl}\omega_{il} + \sigma_{il}\omega_{jl} \tag{18}$$

in which $\omega_{ij} = \frac{1}{2}(\dot{x}_{i,j} - \dot{x}_{j,i})$ is the spin tensor, and σ_{ij}^{∇} is the Jaumann stress rate and determined from the strain rate $\dot{\varepsilon}_{ij} = \frac{1}{2}(\dot{x}_{i,j} + \dot{x}_{j,i})$ by a constitution model.

strain rate of particle p is calculated by using updated velocity

$$\dot{\varepsilon}_{pij} = \frac{1}{2}\sum_{h=1}^{8}\left(v_{hi}^{k+1}N_{hp,j}^{k} + v_{hj}^{k+1}N_{hp,i}^{k}\right) \tag{19}$$

where velocities at grid nodes are mapped back from the updated particle velocities by $v_{hi}^{k+1} = \sum_{p=1}^{n_p} M_p v_{pi}^{k+1} N_{hp}^{k}/m_h^k$.

2.2 GIMP

One of the defects of original MPM is that when a particle crosses computational grid cell during deformation, stress oscillation which was identified as cell crossing noise can be generated. [6] developed Generalized Interpolation Material Point (GIMP) method which is an extension of the original MPM.

The GIMP method is based on Petrov-Galerkin discretization scheme. By introducing particle characteristic function $\chi_p(x)$, physical variables can be approximated as

$$f(x) = \sum_p f_p \chi_p(x) \tag{20}$$

where subscript p indicates variable carried by particle. Using Eq. (20) to represent density and stress , and substituting Eq. (6) for displacement in Eq. (4), discrete formulation analogue to Eq. (10) can be obtained, where N_{hp} and $N_{hp,j}$ in original MPM formulation are replaced by

$$S_{hp} = \frac{1}{V_p}\int_{\Omega_p\cap\Omega} \chi_p(x) N_h(x)\mathrm{d}\Omega \tag{21}$$

$$S_{hp,j} = \frac{1}{V_p}\int_{\Omega_p\cap\Omega} \chi_p(x) N_{h,j}(x)\mathrm{d}\Omega \tag{22}$$

By choosing different particle characteristic function and grid shape function as trial and test function respectively, different GIMP methods can be obtained. The original MPM is recovered when Delta function is used as particle characteristic function, namely

$$\chi_p(x) = \delta(x - x_p)V_p \tag{23}$$

and the finite element shape function Eq. (8) is used as grid shape function. If the particle characteristic function is replaced by

$$\chi_p(x) = \begin{cases} 1 & x \in \Omega_p \\ 0 & x \notin \Omega_p \end{cases} \tag{24}$$

which indicate a particle represent a continuous block of material, the contiguous particle GIMP method mentioned in [[6]] can be obtained. For one dimentional problem, assuming two particles are initially placed in one cell and the particle size remain constant during deformation process, Eq. (21) for contiguous particle GIMP can be simplified to

$$S(\xi) = \begin{cases} \frac{7-16\xi^2}{8} & \xi \leqslant 0.25 \\ 1-\xi & 0.25 < \xi \leqslant 0.75 \\ \frac{(5-4\xi)^2}{16} & 0.75 < \xi \leqslant 1.25 \\ 0 & \xi > 1.25 \end{cases} \tag{25}$$

where $\xi = |\frac{x_p - x_h}{d_c}|$, d_c is the cell size. For three dimension problem, $S_{hp}(x) = S(\xi)S(\eta)S(\zeta)$. This simplified version of contiguous particle GIMP method is equivalent to the GIMP method which takes Delta function as particle characteristic function and Eq. (25) as grid shaped function.

The approximation function in GIMP could have continuous derivative (in contrast to C^0 continuous finite element shape function used in MPM). The computational cost is increased, but GIMP method benefits the precision and stability. So called crossing cell noise can be suppressed as demonstrated in [[6, 41]] and the numerical examples in this paper.

2.3 Contact simulation in MPM

The positions of the material points are updated by moving them in the single-valued, continuous velocity field that arises from the mapping through element shape functions. The velocity field is single-valued in MPM so that the interpenetration of material is precluded when two bodies contact. Therefore no-slip contact condition between two contact bodies is automatically satisfied. Contact algorithms with slip and friction have been proposed to simulate granular material in which friction between granules should be considered [[5, 33]].

As for explosion problems in which the deformation process has very high strain rate and complete in a very short time period, the slip effect between explosion products and surrounding material can be omitted. No matter whether the materials are fluids or solids, they are discretized to a set of material points. Therefore, interaction between explosive products and surrounding material can be simulated using MPM in a single domain without additional treatment of the contact interface.

3 Adaptive particle splitting scheme

Numerical fracture was observed in SPH simulation because of tensile instability [[18]]. Although MPM is stable under tensile stress state, numerical fracture still

exist under some circumstances. In fact, fracture occurs when the space between two particles is greater than the length of a grid cell in MPM simulation [[42]]. This feature can be used as a rough simulation of fracture in hyper velocity impact simulations. However in the problems with extreme expansion and stretching, such as in the explosion and shaped charge problems, material usually undergoes extreme large ductile deformation without fracture. Solid material behaves like fluid in jet formation process. Plastic flow produce an elongation in one direction and shortening in the perpendicular direction in jet stretching. So particle rearrangement or adding new particles is necessary to provide adequate description of deformation. A modified MPM [[31]], which is named as lagrangian integration point finite element method, has been used to simulate viscoelastic materials in geological modeling. A scheme of splitting integration point was proposed by using lightweight ghost particles to track the bounds of volume associated with particles. In MPM formulation addressed in this paper, the strain can be calculated explicitly in each time step, so that the accumulated strain of the particle can be used directly in the splitting criterion. The detailed scheme is summarized as follows.

Particle carries all the parameters including density and particle volume in MPM. Therefore, the variables carried by a particle can be used to determine the particle splitting criterion. Accumulated strain in ith direction, ε_i, can be calculated as

$$\varepsilon_i = \sum_{k=1}^{N} \Delta\varepsilon_i^k = \sum_{k=1}^{N} \dot{\varepsilon}_{ii}^k \Delta t \tag{26}$$

where k is the time step counter, $\Delta\varepsilon_i$ is the strain increment calculated by using the strain rate acquired in Eq. (19). The equivalent length of a particle in ith direction is defined by

$$L_i = L_0(1+\varepsilon_i) \tag{27}$$

where $L_0 = \sqrt[3]{m_p/\rho_0}$ is the initial particle length, $(1+\varepsilon_i)$ indicates the extension of the particle in ith direction. The adaptive splitting criterion can be specified as

$$L_i > \alpha d_c \tag{28}$$

where α is a user provided adaptive factor and d_c is the cell length. The value of α is usually less than 1.0 to ensure appropriate number of particles in each cell. If the equivalent length of the particle meets the criterion, the particle will be split into two particles as shown in Fig.1.

The distance between two split particles is set to $0.5\alpha d_c$. When a particle is split, the variables associated with the amount of material, such as mass m_p, volume,

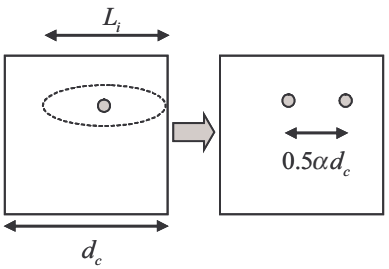

Figure 1: Adaptive particle splitting scheme

internal energy, are halved and then assigned to each new particles. Other variables such as stress, strain and temperature are assigned to new particles directly. Accumulated strain ε_i of new particles is determined according to the requirement

$$L_i' = \begin{cases} 0.5L_i & \text{in split direction} \\ L_i & \text{in other two directions} \end{cases} \tag{29}$$

where L_i' denote the equivalent length of new particles after split. Note that the mass of new particles is half of the original mass m_p, $L_0' = \sqrt[3]{0.5}L_0$. Substituting the equivalent length defined in Eq. (27) into Eq.(29), the adjusted accumulated strain can be obtained as

$$\varepsilon_i' = \begin{cases} 0.63\varepsilon_i - 0.37 & \text{in split direction} \\ 1.26\varepsilon_i + 0.26 & \text{in other two directions} \end{cases} \tag{30}$$

4 Numerical implementation

In order to stabilize and capture the shock wave, artificial bulk viscosity [[13]] is included by replacing p in momentum equations by $p+q$ in order to treat shock waves, where the viscosity term

$$q = \begin{cases} c_0\rho l_e^2 (\dot{\varepsilon}_{kk})^2 - c_1\rho l_e c\dot{\varepsilon}_{kk} & \dot{\varepsilon}_{kk} < 0 \\ 0 & \dot{\varepsilon}_{kk} \geqslant 0 \end{cases} \tag{31}$$

where l_e is the characteristic length, and is replaced by cell length d_c in MPM simulation. $\dot{\varepsilon}_{kk}$ is the bulk strain rate, c is the sound speed, c_0 and c_1 are dimensionless constants whose default values are 1.5 and 0.06 respectively.

Johnson-Cook material model [[17]] is implemented in MPM3DPP code, in which the equivalent flow stress is expressed as

$$\sigma_y = (A + B\varepsilon^n)(1 + C\ln\dot{\varepsilon}^*)(1 - T^{*m}) \tag{32}$$

where ε is the equivalent plastic strain, $\dot{\varepsilon}^* = \dot{\varepsilon}/\dot{\varepsilon}_0$ is the dimensionless plastic strain rate for $\dot{\varepsilon}_0 = 1.0\,\mathrm{s}^{-1}$ and $T^* = (T - T_{\mathrm{room}})/(T_{\mathrm{melt}} - T_{\mathrm{room}}) \in [0,1]$ is the homologous temperature. A, B, n, C and m are the material constants. Strain rate hardening effect and thermal softening effect of material under impact loading are take into account in Johnson-Cook model.

During the metal deformation precess, such as copper jet formation process in shaped charge problem, irreversible plastic deformation occurred and the plastic work was converted to heat which contribute to temperature raising. Considering that time span of process is small and adiabatic conditions prevail, the heat conduction could be omitted. So the equation connecting temperature raising and plastic work takes the form [[28]]

$$\rho c_p \dot{T} = \beta \dot{W}^p \tag{33}$$

where ρ is the density, c_p is the heat capacity, W^p is the plastic work, β is the material parameter which is the conversion fraction of work rate to heat rate. β may depend strongly upon strain and strain rate for some material [[28]], but β is often simply assumed to be a constant in the range $0.85 - 1.00$. Usually $\beta = 0.9$ is an acceptable approximation for most metals according to Meyers [[29]]. Temperature is calculated by accumulate temperature increment and is used in the Johnson-Cook model to account for thermal softening.

The pressure is updated by a equation of state for both gaseous material and solid material under high pressure. The Mie-Grüneisen equation of state [[13]] is implemented in MPM3DPP for solid material. With the assumption of linear relationship between shock wave velocity U_s and particle velocity U_p, $U_s = C + SU_p$, the pressure of solid material is updated by

$$p = \begin{cases} p_H \left(1 - \dfrac{\gamma\mu}{2}\right) + \gamma_0 E & \mu \geqslant 0 \\ \rho_0 c_0^2 \mu + \gamma_0 E & \mu < 0 \end{cases} \tag{34}$$

where

$$p_H = \frac{\rho_0 c_0^2 \mu (1+\mu)}{[1-(S-1)\mu]^2} \tag{35}$$

The subscript H refers to the Hugoniot curve, $\mu = \rho/\rho_0 - 1$ is used to represent the compression and γ is the Grüneisen parameter, $\gamma\rho = \gamma_0\rho_0$.

The ideal gas law is used as the equation of state for gas under pressure

$$p = (\gamma - 1)\frac{\rho}{\rho_0} E \tag{36}$$

where γ is the ratio of specific heats. For the diatomic molecules comprising gas, this coefficient is $\gamma = 1.4$.

The explosion usually includes two processes: the detonation process, and the following process including expansion of gaseous products and its interaction to the surrounding material. The detonation process consists of burning effects and propagation of reactive wave with constant velocity inside the explosive, which is very fast. It only takes few microseconds for the explosive to be burned. Two different detonation can be used, programmed burn based on time, or compression burned where detonation is based on material compression. After detonation, the produced gas is governed by the equation of state. In programmed burn, the detonation wave is assumed to travel at detonation velocity.

Jones-Wilkins-Lee(JWL) equation of state [[43]] is widely used for describing the detonation products

$$p = A(1 - \frac{\omega}{R_1 V})e^{-R_1 V} + B(1 - \frac{\omega}{R_2 V})e^{-R_2 V} + \frac{\omega E}{V} \tag{37}$$

where $V = v/v_0$ is the relative volume. A, B, R_1, R_2 and ω are the material constants for specified explosive. E in (34), (37) and (36) is internal energy per initial volume.

5 Numerical examples

5.1 TNT slab detonation

A 10-cm long slab of TNT is detonated from one end which has fixed wall. The detonation wave travels to the other end at the detonation speed. This problem has been studied numerically by using finite element method [[35]] and SPH [[22]] respectively and can be taken as benchmark problems to validate the codes simulating high explosive. MPM and SPH show different characters in simulation of shock related problems [[26]], original MPM is efficient but noisy and need to suppress the numerical noise by using the artificial bulk viscosity and GIMP.

In this simulation, TNT is used as the high explosive which has density of $1630\ \mathrm{kg/m^3}$ and detonation velocity of $6930\ \mathrm{m/s}$. The parameters of JWL equation of state are taken from [[21]] as $A = 3.712 \times 10^{11}\ \mathrm{N/m^2}$, $B = 0.0321 \times 10^{11}\ \mathrm{N/m^2}$, $R_1 = 4.15$, $R_2 = 0.95$, $\omega = 0.3$, energy per intial volume $E_0 = 6993 \times 10^6\ \mathrm{J/m^3}$.

MPM3DPP is a three dimensional MPM code. To analyze this one dimension problem, the particles are totally constrained in y and z directions. In our simulation, 2000 particles are initially located in 1000 cells. MPM results are compared with LS-DYNA results in Fig. 2, in which the MPM results data are collected from grid nodes. Fig. 2 shows good agreement between pressure profiles obtained by MPM3DPP and LS-DYNA. C-J pressure determined from experimental results is

21 GPa which is illustrated as the dashed line. The peak pressure obtained by MPM3DPP is very close to the experimental C-J pressure.

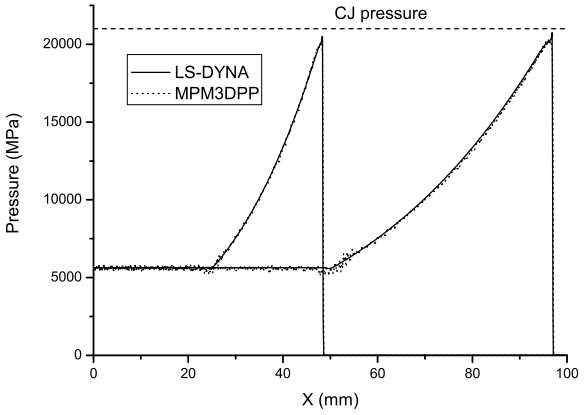

Figure 2: TNT slab detonation, 7μs and 14μs

There are two sources of numerical oscillation, cell crossing induced and shock wave induced. Both of them are successfully decreased by using GIMP option and artificial bulk viscosity. The constants for viscosity are set as $c_0 = 3.0$ and $c_1 = 0.2$.

5.2 Shock tube problem

Shock tube problem which has an analytical solution is often used to test the capability of code on simulating compressible fluid. Sod's model problem [[36]] is regarded as a standard test. This shock tube problem consists of a shock tube where a diaphragm separates two regions which have different densities and pressures. The gas in two regions are initially at rest. The initial densities and pressures are $\rho_1 = 1.0$, $p_1 = 1.0$, $\rho_2 = 0.125$, $p_2 = 0.1$. At time $t > 0$ the diaphragm is broken. Then the shock and the contact interface travel at different speed from left to right. The results usually plotted at $t = 0.143$ when shock travels a distance of about 0.25.

Two particles are located in each cell initially. The velocity profiles with and without adaptive splitting are compared in Fig. 3. Totally 400 particles are evenly distributed initially and the number of particles are increased in the expansion area of left part. The number of particles raised from 400 to 556 by setting adaptive factor $\alpha = 0.55$. Simulation result successfully recover the analytical solution with GIMP option, but oscillation still exist due to insufficient particles in expansion area if no adaptive split scheme is used. The result can be improved by collocate more particles manually in expansion region [[26]]. However, better solution can be automatically achieved with less particles by using adaptive scheme. The refined case

use 1000 cells and initially 2000 particles evenly distributed in the computational domain. 2661 particles are finally in the domain at $t = 0.143$ by using adaptive scheme. The profile fits very well with the analytical solution.

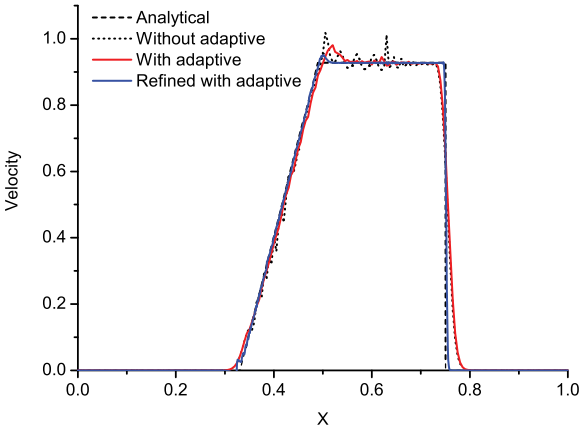

Figure 3: Velocity profile of shock tube at t = 0.143

5.3 Explosively driven flyer

To validate the capability of MPM3DPP code in simulating interaction between detonating explosive with surrounding material, an explosively driven metal flyer was analyzed.

A steel plate accelerated by TNT explosive is examined in this example. The plate is placed beside the explosive charge as illustrated in Fig.4 and the explosive is detonated synchronously from the other side. Two computational models, the infinite plate model and the finite plate model, are used in MPM simulation. The one dimensional model is set as previous example to simulate the infinite plate. The two dimensional model uses one layer of material points and confining the deformation in perpendicular direction. The plate with finite size in the lateral direction can be studied with this two dimensional model as shown in Fig.4.

The expected terminal velocity of the explosively driven flyer can be calculated according to empirical equations. The Gurney equation [[29]] is simple and has been proven to be reliable in predicting the terminal velocity of explosively accelerated devices. The ratio of terminal flyer velocity V to the characteristic velocity $\sqrt{2E}$ is an explicit function of the ratio of metal mass to explosive charge mass M/C in the Gurney equation. $\sqrt{2E}$ is also known as the Gurney energy, and has different values for various explosives. $\sqrt{2E} = 2.37$ mm/μs for TNT. Considering the

open-face sandwich case, the terminal flyer velocity can be expressed as

$$V = \sqrt{2E}\left[\frac{3}{1+5(M/C)+4(M/C)^2}\right]^{\frac{1}{2}} \tag{38}$$

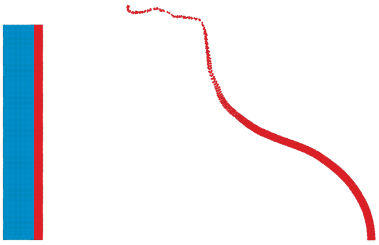

Figure 4: Explosively driven flyer, initial configuration and flyer deformation at 250 μs after detonation.

The simulated flyer velocities are acquired by averaging particle velocities through plate thickness. Since the Gurney equation only predict the terminal plate velocity, the termination time of the simulation is set to be long enough during which the acceleration process finishes. The results acquired by MPM3DPP simulation with various M/C ratios are compared with the Gurney equation (38) in Fig.5.

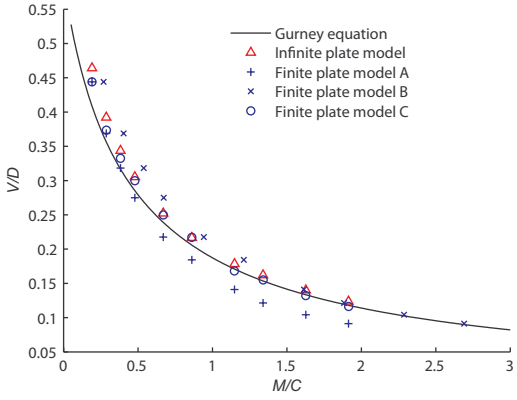

Figure 5: The terminal flyer velocity with various M/C ratios.

The simulation results are generally in good agreement with Gurney equation. Different computational models lead to some variance. Results of infinite plate model are generally a bit larger than that estimated by Gurney equation and become close to them when M/C increases. Besides the infinite plate model, three finite plate model with different configurations are examined. Lateral size of the plate is fixed in group A and B. Results of group A are smaller than that of Gurney equation for bigger M/C value because of the lateral effect. Kennedy suggests that the lateral edge of the explosive should be subtracted from the total mass C with an angle of 30 degree to take the lateral effect into consideration. The results in group B are acquired by applying mass modification based on the results in group A. The results with mass modification fit well with that of Gurney equation in large M/C region, but seem to be over modified in small M/C region. The results in group C are obtained by setting the plates with constant length-to-thickness ratio. The ratio is set to be 50 which is equal to the largest value in group A. Group C shows the best fitness with Gurney equation. Note that the Gurney equation is derived under the infinite plate assumption and the Gurney energy is determined by experiments. Therefore, it is reasonable that the simulation results with relative thin plate fit better with Gurney equation.

The MPM simulation gives not only the terminal velocity but also the whole acceleration process and the deformation of the plate flyer as illustrated in Fig.4. More referential data are given by the MPM simulation than by the Gurney equation.

MPM with adaptive splitting scheme applied to explosive is also examined for infinite plate model. The terminal velocities become a little larger with adaptive option, but the maximum deviation is less than 1%. Since the results in this example are not sensitive to the adaptive option, only results without adaptivity is illustrated in Fig.5.

5.4 Shaped charge jet formation

Linear shaped charge which can be simplified as two dimensional plane strain problem is considered. The liner collapse and jet formation process is examined. MPM3DPP is used by setting one layer of material points as mentioned in previews example to simulate this two dimensional problem . The initial configuration of shaped charge is illustrated in Fig. 6. Only half of the shaped charge is simulated by considering the symmetry. The apex angle α is 38 degree. The explosive is TNT and the same JWL parameters are used as in the first case. The outer shell and the liner consist of copper. The material parameters of Johnson-Cook model and Grüneisen EOS for copper are listed in the Table.1.

Planar detonation, in which the detonation initiated synchronously from the end without liner, is employed. Fig.7 compares the difference of jet formation results

Table 1: Material parameters of copper

A (MPa)	B (MPa)	n	c	m	
90	292	0.31	0.025	1.09	
ρ (kg/m^3)	E (GPa)	ν	C (m/s)	S	γ_0
8930	117	0.35	3300	1.49	1.96

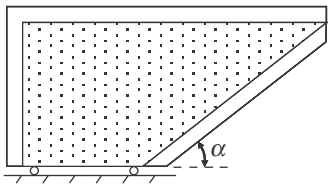

Figure 6: Initial configuration of shaped charge.

acquired by MPM and adaptive MPM. The numerical fracture is avoid by using adaptive splitting scheme. It worth noting that GIMP option and adaptive option for explosive material do not affect the final configuration much in this case. So adaptive option is only applied to copper liner.

Figure 7: Jet configuration at t = 30 μs, MPM results on the top encounter numerical fracture and adaptive MPM results on the bottom avoid that problem. Particles that represent explosion products are removed for clarity.

Jet tip velocity and slug velocity can be obtained by theoretical estimation with the model proposed by Birkhoff et al. see [[29]]. In their theoretical model, the liner is treated as inviscid, incompressible fluid and a steady-state collapse model is assumed. The jet velocity is mainly affected by ratio of liner mass to explosive mass and apex angle. According to theoretical estimation mentioned in [29], the jet tip velocity is 3.7 km/s and slug velocity is 0.6 km/s in this case. Fig.8 shows the

distribution of velocity in x direction at time of 21 μs simulated by using MPM. The velocity results obtained by simulation are in good agreement with the theoretical estimations. It is showed in Fig.8 that the highest temperature of jet appears at jet tip and center of the jet column where the material deforms the most. The maximum temperature is about 1500 K to 1800 K. The main part of copper jet is still in solid state according to the calculation.

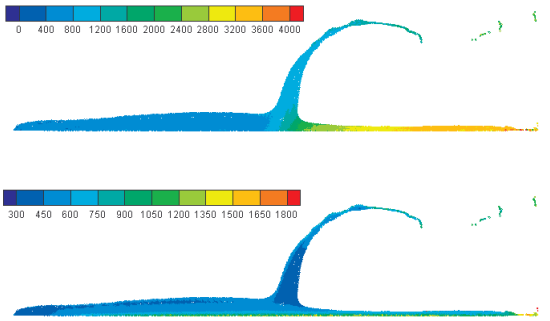

Figure 8: Velocity distribution (top) and temperature distribution (bottom) at t = 21 μs.

5.5 3D shaped charge

Three dimensional shaped charge problem consist of a cone liner and cylinder charged explosive. The geometric model is axisymmetric and the cross section geometry is the same as Fig.6. The apex angle is also the same but the ratio of liner mass to explosive mass is different from previous example. The jet tip velocity and slug velocity predicted by theoretical formula are 4.1 km/s and 0.7 km/s. Configuration of jet formation with distribution of velocity in jet direction is illustrated in Fig.9. The jet velocity and slug velocity are roughly consistent with theoretical estimation.

6 Conclusion

A three dimensional MPM code, MPM3DPP, is developed, in which GIMP shape function is implemented. Several material models and equation of states are implemented to simulate different solid and gas material. MPM provide a convenient approach to simulate high explosive explosion and the consequent driving or propelling effect to the surrounding material in a single domain without addition treatment to the interface.

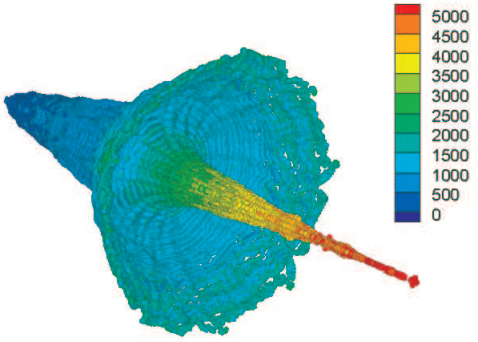

Figure 9: Velocity distribution of 3D shaped charge jet formation at t = 20 μs.

By introducing adaptive particle splitting scheme, numerical noise due to insufficient particles in grid cell can be suppressed and numerical fracture in MPM simulation can be avoided. Numerical examples show that MPM is an effective tool in simulating explosive detonation, explosion product expansion. Compared with empirical formula, such as Gurney equation, MPM simulation gives good fitting in terminal velocity and furthermore can provide the whole deformation process with different configurations. MPM also shows that it is an prospective tool in engineering applications such as shaped charge jet formation problem.

Acknowledgement: This work was supported by the National Science Foundation of China under grant 10872107, and the Science Foundation of Computational Physics, IAPCM, China.

References

[1]**Alia, A.; Souli, M.** (2006): High explosive simulation using multi-material formulations. *Applied Thermal Engineering*, vol. 26, pp. 1032–1042.

[2]**Atluri, S. N.** (2004): *The Meshless Method(MLPG) for Domain & BIE Discretizations*. Tech Science Press.

[3]**Atluri, S. N.; Zhu, T.** (1998): A new meshless local petrov-galerkin (mlpg) approach in computational mechanics. *Computational Mechanics*, vol. 22, no. 2, pp. 117–127.

[4]**Bardenhagen, S. G.; Brackbill, J. U.; Sulsky, D.** (2000): The material-point method for granular materials. *Computer Methods in Applied Mechanics and Engineering*, vol. 187, no. 3-4, pp. 529–541.

[5]**Bardenhagen, S. G.; Guilkey, J. E.; Roessig, K. M.; Brackbill, J. U.; Witzel, W. M.; Foster, J. C.** (2001): An improved contact algorithm for the material point method and application to stress propagation in granular material. *CMES-Computer Modeling in Engineering & Sciences*, vol. 2, no. 4, pp. 509–522.

[6]**Bardenhagen, S. G.; Kober, E. M.** (2004): The generalized interpolation material point method. *CMES-Computer Modeling in Engineering & Sciences*, vol. 5, no. 6, pp. 477–495.

[7]**Belytschko, T.; Krongauz, Y.; Organ, D.; Fleming, M.; Krysl, P.** (1996): Meshless methods: An overview and recent developments. *Computer Methods in Applied Mechanics and Engineering*, vol. 139, no. 1-4, pp. 3–47.

[8]**Belytschko, T.; Liu, W. K.; Moran, B.** (2000): *Nonlinear Finite Elements for Continua and Structures*. John Wiley & Sons.

[9]**Brackbill, J. U.; Kothe, D. B.; Ruppel, H. M.** (1988): Flip: a low-dissipation, particle-in-cell method for fluid flow. *Computer Physics Communications*, vol. 48, pp. 25–38.

[10]**Brown, R. E.; Majerus, M. E.; Lewis, J. S.** (1995): Building characteristics into a shaped charge to achieve unique performance requirements. *International Journal of Impact Engineering*, vol. 17, pp. 121–130.

[11]**Daphalapurkar, N. P.; Lu, H.; Coker, D.; Komanduri, R.** (2007): Simulation of dynamic crack growth using the generalized interpolation material point (gimp) method. *International Journal of Fracture*, vol. 143, no. 1, pp. 79–102.

[12]**Guo, Y. J.; Nairn, J. A.** (2006): Three-dimensional dynamic fracture analysis using the material point method. *CMES-Computer Modeling in Engineering & Sciences*, vol. 16, no. 3, pp. 141–155.

[13]**Hallquist, J. O.** (1998): *LS-DYNA Theoretical Manual*. Livermore Software Technology Corporation.

[14]**Han, Z. D.; Liu, H. T.; Rajendran, A. M.; Atluri, S. N.** (2006): The application of meshless local petrov-galerkin (mlpg) approaches in high speed

impact, penetration and perforation problems. *CMES: Computer Modeling in Engineering & Science*, vol. 14, pp. 119–128.

[15]**Han, Z. D.; Rajendran, A. M.; Atluri, S. N.** (2005): Meshless local petrov-galerkin (mlpg) approaches for solving nonlinear problems with large deformations and rotations. *CMES-Computer Modeling in Engineering & Sciences*, vol. 10, no. 1, pp. 1–12.

[16]**Hu, W. Q.; Chen, Z.** (2006): Model-based simulation of the synergistic effects of blast and fragmentation on a concrete wall using the mpm. *International Journal of Impact Engineering*, vol. 32, no. 12, pp. 2066–2096.

[17]**Johnson, G. R.; Holmquist, T. J.** (1988): Evaluation of cylinder-impact test data for constitutive model constants. *Journal of Applied Physics*, vol. 64, no. 8, pp. 3901–3910.

[18]**Johnson, G. R.; Stryk, R. A.; Beissel, S. R.** (1996): Sph for high velocity impact computations. *Computer Methods in Applied Mechanics and Engineering*, vol. 139, no. 1-4, pp. 347–373.

[19]**Lee, W. H.** (2006): *Computer Simulation of Shaped Charge Problems*. World Scientific.

[20]**Li, S.; Liu, W. K.** (2002): Meshfree and particle methods and their applications. *Applied Mechanics Reviws*, vol. 55, no. 1, pp. 1–34.

[21]**Liu, M. B.; Liu, G. R.; Lam, K. Y.; Zong, Z.** (2003): Meshfree particle simulation of the detonation process for high explosives in shaped charge unlined cavity configurations. *Shock Waves*, vol. 12, no. 6, pp. 509–520.

[22]**Liu, M. B.; Liu, G. R.; Zong, Z.; Lam, K. Y.** (2003): Computer simulation of high explosive explosion using smoothed particle hydrodynamics methodology. *Computers & Fluids*, vol. 32, no. 3, pp. 305–322.

[23]**Liu, Y.; Zhang, X.; Sze, K. Y.; Wang, M.** (2007): Smoothed molecular dynamics for large step time integration. *CMES-Computer Modeling in Engineering & Sciences*, vol. 20, no. 3, pp. 177–191.

[24]**Love, E.; Sulsky, D. L.** (2006): An unconditionally stable, energy-momentum consistent implementation of the material-point method. *Computer Methods in Applied Mechanics and Engineering*, vol. 195, no. 33-36, pp. 3903–3925.

[25]**Ma, J.; Liu, Y.; Lu, H. B.; Komanduri, R.** (2006): Multiscale simulation of nanoindentation using the generalized interpolation material point (gimp)

method, dislocation dynamics (dd) and molecular dynamics (md). *CMES-Computer Modeling in Engineering & Sciences*, vol. 16, no. 1, pp. 41–55.

[26]**Ma, S.; Zhang, X.; Qiu, X. M.** (2009): Comparison study of mpm and sph in modeling hypervelocity impact problems. *International Journal of Impact Engineering*, vol. 36, pp. 272–282.

[27]**Ma, T. B.; Wang, C.; Ning, J. G.** (2008): Multi-material eulerian formulations and hydrocode for the simulation of explosions. *CMES-Computer Modeling in Engineering & Sciences*, vol. 33, no. 2, pp. 155–178.

[28]**Mason, J. J.; Rosakis, A. J.; Ravichandran, G.** (1994): On the strain and strain-rate dependence of the fraction of plastic work converted to heat - an experimental-study using high-speed infrared detectors and the kolsky bar. *Mechanics of Materials*, vol. 17, no. 2-3, pp. 135–145.

[29]**Meyers, M. A.** (1994): *Dynamic Behavior of Materials*. John Wiley & Sons.

[30]**Molinari, J. F.** (2002): Finite element simulation of shaped charges. *Finite Elements in Analysis and Design*, vol. 38, no. 10, pp. 921–936.

[31]**Moresi, L.; Dufour, F.; Muhlhaus, H. B.** (2003): A lagrangian integration point finite element method for large deformation modeling of viscoelastic geomaterials. *Journal of Computational Physics*, vol. 184, no. 2, pp. 476–497.

[32]**Ning, J. G.; Chen, L. W.** (2004): Fuzzy interface treatment in eulerian method. *Science in China Series E-Engineering & Materials Science*, vol. 47, no. 5, pp. 550–568.

[33]**Pan, X. F.; Xu, A. G.; Zhang, G. C.; Zhang, P.; Zhu, J. S.; Ma, S.; Zhang, X.** (2008): Three-dimensional multi-mesh material point method for solving collision problems. *Communications in Theoretical Physics*, vol. 49, no. 5, pp. 1129–1138.

[34]**Randles, P. W.; Libersky, L. D.** (1996): Smoothed particle hydrodynamics: Some recent improvements and applications. *Computer Methods in Applied Mechanics and Engineering*, vol. 139, no. 1-4, pp. 375–408.

[35]**Shin, Y. S.; Chisum, J. E.** (1997): Modeling and simulation of underwater shock problems using coupled lagrangian-eulerian analysis approach. *Shock and Vibration*, vol. 4, no. 1, pp. 1–10.

[36]**Sod, G. A.** (1978): A survey of several finite difference methods for systems of nonlinear hyperbolic conservation laws. *Journal of Computational Physics*, vol. 27, pp. 1–31.

[37]**Sulsky, D.; Chen, Z.; Schreyer, H. L.** (1994): A particle method for history-dependent materials. *Computer Methods in Applied Mechanics and Engineering*, vol. 118, no. 1-2, pp. 179–196.

[38]**Sulsky, D.; Schreyer, H. L.** (1996): Axisymmetric form of the material point method with applications to upsetting and taylor impact problems. *Computer Methods in Applied Mechanics and Engineering*, vol. 139, no. 1-4, pp. 409–429.

[39]**Sulsky, D.; Zhou, S. J.; Schreyer, H. L.** (1995): Application of a particle-in-cell method to solid mechanics. *Computer Physics Communications*, vol. 87, no. 1-2, pp. 236–252.

[40]**Tran, L. B.; Udaykumar, H. S.** (2004): A particle-level set-based sharp interface cartesian grid method for impact, penetration, and void collapse. *Journal of Computational Physics*, vol. 193, no. 2, pp. 469–510.

[41]**Wallstedt, P. C.; Guilkey, J. E.** (2007): Improved velocity projection for the material point method. *CMES-Computer Modeling in Engineering & Sciences*, vol. 19, no. 3, pp. 223–232.

[42]**Zhang, X.; Sze, K. Y.; Ma, S.** (2006): An explicit material point finite element method for hyper-velocity impact. *International Journal for Numerical Methods in Engineering*, vol. 66, no. 4, pp. 689–706.

[43]**Zukas, J.; Walters, W.** (1998): *Explosive Effects and Applications*. Spinger.